Amyloid Fibril Solubility

L. G. Rizzi[1] and S. Auer[1,*]

[1]School of Chemistry, University of Leeds, Leeds LS2 9JT, United Kingdom

(Dated: December 11, 2015)

It is well established that amyloid fibril solubility is protein specific, but how solubility depends on the interactions between the fibril building blocks is not clear. Here we use a simple protein model and perform Monte Carlo simulations to directly measure the solubility of amyloid fibrils as a function of the interaction between the fibril building blocks. Our simulations confirms that the fibril solubility depends on the fibril thickness and that the relationship between the interactions and the solubility can be described by a simple analytical formula. The results presented in this study reveal general rules how side-chain side-chain interactions, backbone hydrogen bonding and temperature affect amyloid fibril solubility, which might prove a powerful tool to design protein fibrils with desired solubility and aggregation properties in general.

arXiv:1512.03247v1 [physics.bio-ph] 10 Dec 2015

INTRODUCTION

The maintenance of proteins in their soluble state is crucial to protein homeostasis in living organisms because small changes in their concentration can lead to amyloid-related diseases[1,2]. At a given temperature, the solubility C_e (also known as the "critical concentration"[3–6]) is the concentration of monomers C at which the solution is saturated, for then the fibrils in solution cannot lengthen or shorten. Its importance for example in protein homeostasis arises, because the fibril solubility determines the concentration at which the fibrils can form, as well as the fibrilallion kinetics[6,7] as it is a central parameter in existing nucleation theories (*e.g.* refs.[4,6,8–11]).

Experimental measurements of fibrils solubilities are intrinsically difficult, because they can be very low[12–18] (typically 0.1-100 μM), and are beyond the detection limit of commonly used techniques for small oligomers and fibrils[19]. Experiments are usually made at high concentrations where fibrils form spontaneously, or in the presence of preformed fibrils, and fibril solubilities can be determined by the ratio of the on and off rates of fibril elongation[13,19]. These experiments show that fibril solubilities can vary strongly with point mutations of the amino acid sequence[20–22], and the fibril structure[23,24].

Theoretically, a statistical mechanical description of the fibril solubility can be obtained in the case of linear aggregation in terms of molecular partition functions (*e.g.* refs.[3,5,25,26]). Also, aggregation propensities might be predicted from protein physicochemical properties by using knowledge-based computational approaches[27–30] but they are not able to distinguish between different fibril structures. The thermodynamic stability of amyloid fibrils has been studied by computer simulations using full-atomistic description of proteins[31,32] but they are restricted to fibrils composed of small peptide fragments and are computationally too costly to be repeated under different conditions to obtain a full phase diagram. Simulations using coarse-grained models to explore the self-assembly of large peptide systems have been performed, but they often determine a kinetic rather than a thermodynamic phase diagram (*e.g.* refs.[33,34]), which have been shown to be fundamentally different[35]. A direct calculation of the fibril solubility has been performed by Auer *et al.*[36,37] that revealed the existence of various metastable fibrillar aggregates and that the fibril solubility depends of fibril thickness. However, such simulations are also too costly and have only been performed for one set of interaction parameters. Computer simulations using a lattice model for proteins have been performed to determine the phase diagram from the peak in the heat capacity, but the interpretation of this in terms of fibril solubility is not clear[38]. Although lattice peptide models have been employed to investigate fibril formation and growth[39–43], they did not provide a general understanding of how amyloid fibril solubility is determined by protein-protein interactions.

A theoretical relationship between the interactions of the building blocks of an aggregate and its solubility can be provided by a combination of the well known van't Hoff equation and the Haas-Drenth (HD) model[44,45] but its applicability has never been verified by computer simulations. In its integrated form, the van't Hoff equation is given by

$$C_e = C_r e^{-\lambda} \quad , \tag{1}$$

where C_r is a reference concentration and $\lambda = L/k_BT$ is the dimensionless latent heat of peptide aggregation into fibrillar aggregates The corresponding latent heat L can be estimated theoretically by the HD model[46] for protein crystals, and λ is given by half the binding energy of peptides in the aggregates.

PEPTIDE MODEL

To test this, we consider a peptide model that was recently used to explore the formation of amyloid fibril networks[47]. In this model, all peptides are considered in their aggregation-prone state and are represented by hexagons on a two-dimensional (2D) lattice with

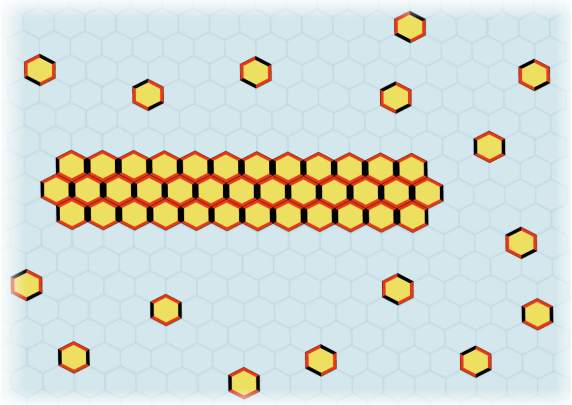

FIG. 1: Illustration of an amyloid fibril composed of three β-sheets. The fibril building blocks (*i.e.* the peptides) are represented by hexagons on a triangular lattice. The four red sides of the hexagons model the hydrophobicity-mediated side-chain side-chain interactions between peptides, while the black sides model directional hydrogen bonds between peptides.

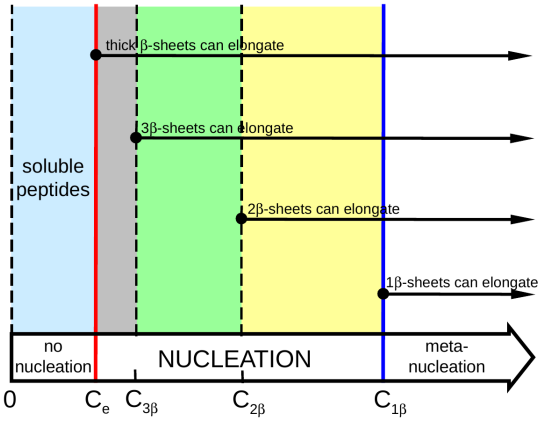

FIG. 2: Concentration ranges showing the fibril solubility C_e, the metanucleation border $C_{1\beta}$, and intermediary concentrations $C_{i\beta}$ for $i \geq 2$.

triangular symmetry, Figure 1. Each hexagon has two opposing strong bonding sides (shown in black) and four weaker bonding sides (shown in red), so that they can self-assemble into a highly ordered cross-β structure characteristic of amyloid fibrils[48,49]. Here the strong bonding sides correspond to hydrogen bonding which drives the formation of β-sheets and the weaker bonding sides correspond to hydrophobicity-mediated side-chain side-chain interactions that drive the fibril thickening.

The corresponding dimensionless surface energies for the strong hydrogen and weak hydrophobicity-mediated bonds can be written as

$$\psi = a\sigma/k_BT = E/2k_BT \tag{2}$$

and

$$\psi_h = a_h\sigma_h/k_BT = E_h/2k_BT \ , \tag{3}$$

respectively. Here σ and σ_h are the corresponding specific surface energies, and a and a_h are the corresponding surface areas of the peptide faces. The second equality results from an approximation between the surface energies and the binding energies E and E_h between peptides. The energy E corresponds to the formation of directional backbone hydrogen bonds, whereas E_h is the energy due to the formation of weaker bonds modeling side-chain hydrophobic interactions between peptides. The fibril solubility in the combined van't Hoff and HD model is then given by

$$C_e = C_r e^{-2\psi-4\psi_h} \ , \tag{4}$$

where we used that the dimensionless latent heat is given by $\lambda = 2\psi + 4\psi_h$.

An important feature characteristic of amyloid fibrils is that their solubility depends on the fibril thickness[11,36,37,40]. It has been shown that the solubility of fibrils composed of $i\beta$-sheet layers is given by[10]($i = 1, 2, 3, \dots$)

$$C_{i\beta} = C_e e^{4\psi_h/i} \ . \tag{5}$$

Substitution of the fibril solubility C_e given by Eq. 4 into Eq. 5 yields ($i = 1, 2, 3, \dots$)

$$C_{i\beta} = C_r e^{-2\psi-4\psi_h(1-1/i)} \ . \tag{6}$$

The analytical expressions given by Eqs. 4 and 6 define the concentration range between the fibril solubility C_e and the threshold concentration $C_{1\beta}$ at the nucleation/metanucleation border (termed also "supercritical concentration"[4,6]) in which fibrils nucleate[10,11]. As illustrated in Figure 2, no fibrils can nucleate when the peptide concentration $C < C_e$, whereas for $C > C_{1\beta}$ the fibril nucleus is a single peptide and fibrils form in the absence of any nucleation barrier[4,10,11,45,50,51]. Importantly, for intermediate concentrations, $C_e < C < C_{1\beta}$, fibril nucleation and elongation depends on their thickness[41]. Despite the fundamental importance of those expressions, they have not yet been verified by neither simulations nor experiments.

SIMULATION DETAILS

To do this we perform Monte Carlo (MC) simulations in which we determine the equilibrium concentration at which a fibril of a fixed thickness neither grows nor shrinks. The simulations are performed on a 2D triangular lattice with 512^2 sites. At the beginning of the simulation one single fibril of fixed thickness i is put in the center of the simulation box and peptide monomers

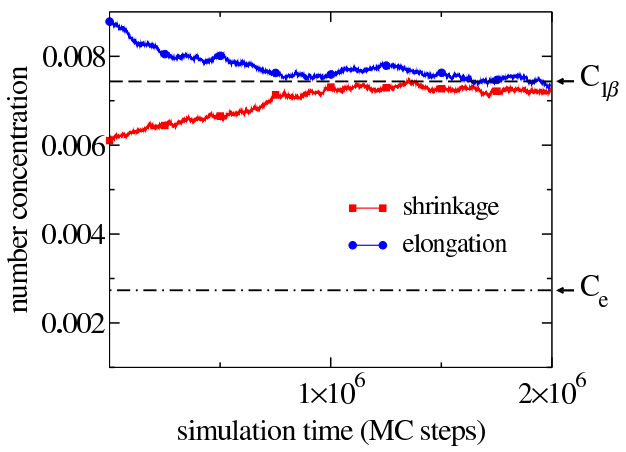

FIG. 3: Solubility measurements for a 1β-sheet fibril showing that, through random attachment and detachment events, the number concentration of peptides in solution approaches the equilibrium concentration $C_{1\beta}$ instead of the solubility C_e. The blue circle and red squares data were obtained from fibril elogantion and fibril schrinkage simulations, respectively. The horizontal dashed and dash-dotted lines are theoretical values predicted, respectively, by Eqs. 6 and 4 considering $\psi = 3$ and $\psi_h = 0.25$.

are randomly placed on the remaining lattice sites (see Figure 1 for a snapshot). In the MC simulations we only perform diffusion-like and rotational moves as described in previous simulations[39,47]. Depending on the peptide concentration the fibril will either elongate or shrink until the equilibrium concentration is reached, as illustrated in Figure 3. We emphasize that during the simulation the fibril can only lengthen and is not allowed to thicken. Typically in each simulation we perform 10^7 MC steps and each solubility measurement is an average over four independent simulations. In the following we present our simulation results for the fibril solubility as a function of the hydrophobicity parameter ψ_h, hydrogen bonding parameter ψ, and temperature to verify the applicability of Eqs. 4 and 6.

RESULTS AND DISCUSSIONS

Weak Hydrophobic Effect. The presence of hydrophobicity-mediated bonds has been shown to be an important factor in the formation of fibrillar aggregates. Fibril structure and point mutations change the interactions between side-chains of the peptides in the fibril and can alter their aggregation propensity[52]. In Figure 4a we present results of the ψ_h dependence of $C_{i\beta}$ at fixed ψ. As can be seen from the figure, $C_{i\beta}$ decreases with increasing ψ_h for all fibrils with a thickness larger than one, and this effect becomes stronger with increasing fibril thickness. The values of $C_{i\beta}$ are given in units of peptides per lattice site. Even though our results have been obtained in 2D, an estimate for the fibril solubilities in 3D can be obtained by scaling them as $C_{i\beta}^{3/2}$. Such scaling implicitly assumes that the interactions of the peptide in the third dimension, and thereby to the latent heat, are negligible. Assuming that the area of the lattice sites is 1 nm^2, the number concentrations in Figure 4a yields threshold concentrations $C_{1\beta}$ in 3D around 1 mM and solubilities C_e in 3D equal to 238 μM for $\psi_h = 0.25$ and 0.1 μM for $\psi_h = 1.5$. Figure 4b shows the same data in a $\ln(C_{i\beta})$-vs-ψ_h plot. A fit of these data points to Eq. 6 with fixed i illustrates the predicted linear dependence with slope $-4(1-1/i)$. Furthermore, a plot of $\ln(C_{i\beta})$-vs-$1/i$ (Figure 4c) can be used to fit Eq. 6, which provides estimates for the solubility C_e in the limit of $i \to \infty$ and the reference concentration C_r. There is good agreement between the estimates for C_e obtained by this scaling analysis and the direct measurements (Figure 4b), and C_r is independent of ψ_h (Figure 4d). We note that the value $C_r \approx 3$ (in units of peptides per lattice site) is related to the number of states that peptides can assume in our lattice model (Figure 1). The reason for this is that only one of the three possible orientations can lead to a successful monomer attachment to the fibril, so that there will be 3 times more monomers in solution than would be if all of them were in the same alignment of the peptides in the fibril. Furthermore, the fact that C_r is independent of ψ_h is important for theoretical studies to predict changes in the solubility as it can be assumed constant (see *e.g.* ref.[45]). Thus, the main effect of decreasing the hydrophobicity-mediated interactions ψ_h is that it increases the solubilities C_e and $C_{i\beta}$ for $i > 1$, but does not alter the metanucleation border $C_{1\beta}$. This rationalizes the experimental observations that amino acid substitutions that decrease the hydrophobicity-mediated interaction between the fibril building blocks decrease its aggregation propensity[20,21,52–54].

Hydrogen Bonding Effect. The lengthening of amyloid fibrils is driven by the formation of backbone hydrogen bonds in the direction of the fibril lengthening axis. The strength of the hydrogen bonding network between neigboring peptides in the fibril varies depending on the amino acid sequence, because it determines the number of hydrogen bonds that can be formed[55]. To determine the effect of changes in the hydrogen bonding interactions we vary ψ while keeping the strength of the hydrophobicity-mediated interactions ψ_h fixed. Figure 5a shows that $C_{i\beta}$ decreases with increasing ψ. A plot of these data as $\ln(C_{i\beta})$-vs-ψ coordinates, illustrates a linear dependence and that the slope is independent of the fibril thickness. Indeed, a fit of Eq. 6 with fixed i to these data points shows that the slope is equal to -2 for all i (Figure 5b). As before, a scaling analysis to obtain the bulk solubility C_e in the limit of $i \to \infty$ and the reference concentration C_r can be obtained by

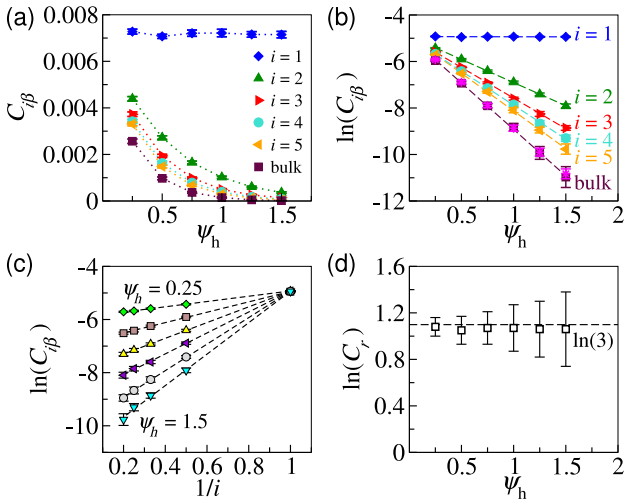

FIG. 4: (a) Dependence of solubilities $C_{i\beta}$ on ψ_h: diamonds, up triangles, right triangles, circles, left triangles - simulation data for 1β, 2β, 3β, 4β, 5β-sheet, respectively; squares - data obtained for a bulk fibril (*i.e.* $i = 100$); dotted lines - guide to the eyes only. (b) monolog plot of the same data presented in (a); dashed lines - best fit of Eq. 6; asterisks - data obtained for $i \to \infty$ from scaling analysis. (c) $\ln(C_{i\beta})$-vs-$1/i$ plot; dashed lines - best fit of Eq. 6. (d) reference concentration C_r obtained from the scaling analysis described in text; dashed line is the $C_r = 3$ line. All results here were obtained for $\psi = 3$ at room temperature, *i.e.* $k_BT = 2.5$ kJ.mol^{-1}.

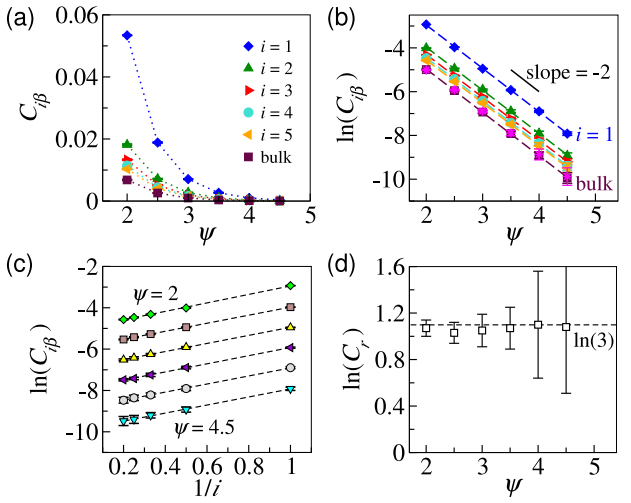

FIG. 5: (a) Dependence of solubilities $C_{i\beta}$ on ψ. Symbols are the same as in Figure 4. Dotted lines are guides to the eyes only. (b) monolog plot of the same data presented in (a); dashed lines - best fit of Eq. 6; asterisks - data obtained for $i \to \infty$ from scaling analysis as described in main text. (c) $\ln(C_{i\beta})$-vs-$1/i$ plot for the scaling analysis; dashed lines - best fit of Eq. 6. (d) reference concentration C_r obtained from the scaling analysis; dashed line - $C_r = 3$ line. All results here were obtained for $\psi_h = 0.5$ and $k_BT = 2.5$ kJ.mol^{-1}.

a fit of Eq. 6 to our data presented in a $\ln(C_{i\beta})$-vs-$1/i$ plot (Figure 5c). As can be seen in Figure 5b, there is again good agreement of the results obtained from our scaling analysis and direct measurements of C_e. Furthermore, also in this case the so obtained reference concentration $C_r \approx 3$ is independent of ψ (Figure 5d). The main effect of decreasing the hydrogen bond energy interaction ψ is that it increases the solubility C_e and the threshold concentration $C_{1\beta}$ while keeping the ratio $C_{1\beta}/C_e$ constant. This effect might explain experiments using hydrogen-deuterium exchange mass spectrometry to demonstrate that the solubilities of different Aβ_{1-40} polymorphs increases as hydrogen bond formation between proteins decreases[23].

Temperature Dependence. Amyloid fibrils are known to have high thermodynamic stability, and the temperatures required for the dissociation of the fibril structure are far greater than needed for *e.g.* the denaturation of native proteins[56]. To test the effect of temperature on the fibril solubility we performed simulations in which the we fixed the binding energies and varied the temperature. Figure 6a illustrates that $C_{i\beta}$ increases with increasing k_BT, and that this effect is less pronounced with the increasing number of fibril layers i. In Figure 6b we present the same data but in a $\ln(C_{i\beta})$-vs-$1/k_BT$ plot. A fit of Eq. 6 with fixed i to these data points using a reference concentration $C_r = 3$ shows a linear dependence with a slope equal to $-(E + 2E_h(1 - 1/i))$ as predicted by Eq. 6. Furthermore, presenting the same data in a $\ln(C_{i\beta})$-vs-$1/i$ plot (Figure 6c), a fit of Eq. 5 to these data points also provides estimates for the solubility C_e from the intercept in the limit of $i \to \infty$. As shown in Figure 6b, such estimates are in good agreement with the direct measurements of C_e for very thick fibrils (*i.e.* for $i = 100$). In the limiting case when $i \to \infty$, the slope obtained for the bulk solubility line C_e corresponds to the latent heat $L = \lambda k_BT$ (Eq. 1), which remarkably is equal to half of the binding energies $E + 2E_h$, as predicted by the HD lattice model (see Figure 6d). The fact that L is half the binding energy cross validates our assumption that $C_r = 3$ in the linear fit of Eq. 5 to the data presented in Figure 6c. Finally, the slopes obtained from the fit of Eq. 5 to data in Figure 6c, in combination with Eq. 3, provide values for the surface energy $a_h\sigma_h$ at each temperature. As shown in Figure 6e, such values are equal to half the values of the weak bond energy $E_h/2$. Furthermore, combined with the estimate for the latent heat λ, the values of $a_h\sigma_h$ can be used to estimate the strong bond surface energies $a\sigma$. Figure 6f confirms that the values of $a\sigma$ are independent of k_BT and equal to half the binding energy of the strong bond $E/2$. Note that the dashed lines in Figs. 6e and f are estimates obtained from the fit of Eq. 6 to data presented in Figure 6 considering $i = 1$. The main effect of increasing the temperature is that it increases both $C_{1\beta}$ and C_e, which is in agreement with experimental measurements of solubilities for a short Aβ-model peptide[57]. In the example presented in Figure 6, increasing the temperature from 10 °C to 60 °C

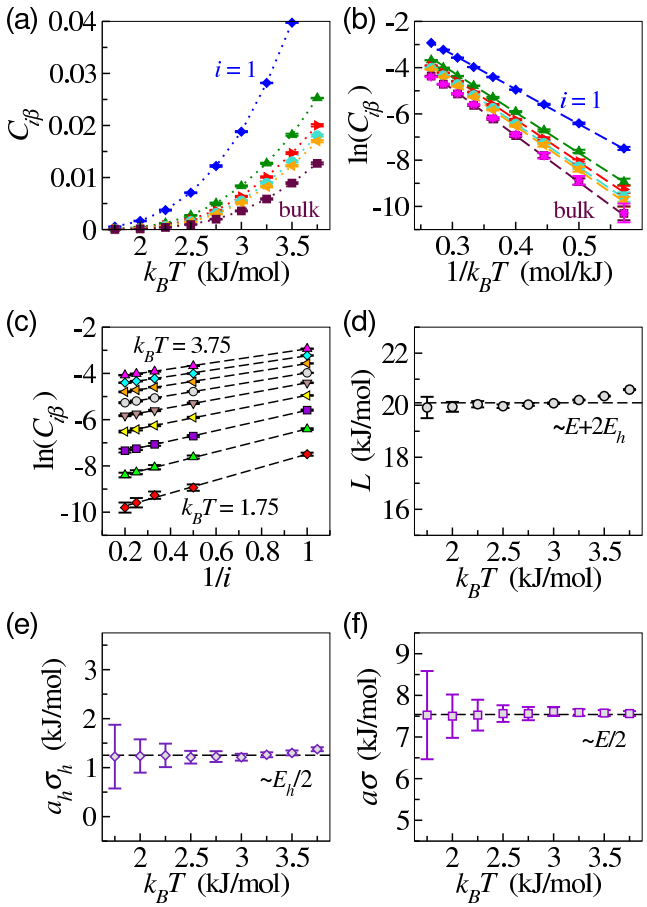

FIG. 6: (a) Dependence of solubilities $C_{i\beta}$ on k_BT. Symbols are the same as in Figure 4. Dotted lines are guides to the eyes only. (b) monolog plot of the same data presented in (a); dashed lines - best fit of Eq. 1 assuming $C_r = 3$; asterisks - data obtained for $i \to \infty$ from the scaling analysis described in main text. (c) $\ln(C_{i\beta})$-vs-$1/i$ plot for the scaling analysis; dashed lines - best fit of Eq. 5 with $C_r = 3$. (d) Specific heat L extracted at each temperature from data in (c) by considering Eqs. 1 and 5 assuming $C_r = 3$; dashed line - estimate of L from the slope of $\ln(C_e)$-vs-$1/k_BT$ in (b) considering Eq. 1. Panels (e) and (f) show, respectively, estimates for the surface energies $a_h\sigma_h$ and $a\sigma$ evaluated from the scaling presented in (a) by considering Eq. 1 and Eq. 5 at each temperature assuming $C_r = 3$; dashed lines in (e) and (f) are estimates extracted from the scaling in (b) for comparison (see text). All results here were obtained for binding energies $E = 15$ kJ.mol^{-1} and $E_h = 2.5$ kJ.mol^{-1}.

changes the solubilities C_e in 3D from 25 μM to 171 μM, and the threshold concentration $C_{1\beta}$ in 3D from 0.61 mM to 2.56 mM, respectively.

CONCLUSIONS

In summary, the main results of the analysis presented is that we numerically verified Eqs. 4 and 6 which provide simple relationships between the solubilities of fibrils of various thickness and the dimensionless specific surface energies that are given by half the dimensionless binding energies between the peptides in the fibril (Eqs. 2 and 3). This is important, as these equations can be used to *e.g.* estimate changes in the fibril solubility upon point mutations or fibril structure. In combination with existing nucleation theories they can also be used to predict how such changes affect their fibrillation kinetics (*e.g.* refs.[44,45]). To design peptides that assemble into fibrils with desired solubility our analysis reveals some general rules: (i) decreasing the hydrophobicity-mediated interaction ψ_h will increase the solubility C_e, corroborating what was previously suggested by experimental studies[20,21,54]; (ii) changes in ψ_h do not alter the value of $C_{1\beta}$, but the solubilities C_e and $C_{i\beta}$ for $i > 1$; (iii) decreasing the hydrogen bond energy interaction ψ will increase both the solubility line C_e and the metanucleation border $C_{1\beta}$ while keeping ratio $C_{1\beta}/C_e$ constant; (iv) higher temperatures increases both $C_{1\beta}$ and C_e.

Finally, we note that our model is limited to peptides in an aggregate-prone state immersed in an implicity athermal solvent; thus neither conformational changes nor solvent effects[57] are considered.

L. G. Rizzi acknowledge support by the Brazilian agency CNPq (Grant N° 245412/2012-3).

* Electronic address: S.Auer@leeds.ac.uk

[1] Vendruscolo, M.; Knowles, T. P. J.; Dobson, C. M. Protein Solubility and Protein Homeostasis: A Generic View of Protein Misfolding Disorders. *Cold Spring Harb. Perspect. Biol.* **2011**, *3*, a010454.

[2] Ciryam, P.; Tartaglia, G. G.; Morimoto, R. I.; Dobson, C. M.; Vendruscolo, M. Widespread Aggregation and Neurodegenerative Diseases Are Associated with Supersaturated Proteins. *Cell Reports* **2013**, *5*, 781.

[3] Hill, T. L. *Linear Aggregation Theory in Cell Biology*; Springer-Verlag New York Inc., 1987.

[4] Powers, E. T.; Powers, D. L. The Kinetics of Nucleated Polymerizations at High Concentrations: Amyloid Fibril Formation Near and Above the "Supercritical Concentration". *Biophys. J.* **2006**, *91*, 122.

[5] Lee, C. F. Self-Assembly of Protein Amyloids: A Competition Between Amorphous and Ordered Aggregation. *Phys. Rev. E* **2009**, *80*, 031922.

[6] Gillam, J. E.; MacPhee, C. E. Modelling Amyloid Fibril Formation Kinetics: Mechanisms of Nucleation and Growth. *J. Phys.: Condens. Matter* **2013**, *25*, 373101.

[7] Schmittschmitt, J. P.; Scholtz, J. M. The Role of Protein Stability, Solubility, and Net Charge in Amyloid Fibril Formation. *Prot. Sci.* **2003**, *12*, 2374.

[8] Jarrett, J. T.; Lansbury, P. T. Seeding "One-Dimensional Crystallization" of Amyloid: A Pathogenic Mechanism in Alzheimer's Disease and Scrapie? *Cell* **1993**, *73*, 1055.

[9] Lomakin, A. L.; Teplow, D. B.; Kirschner, D. A.; Benedek, G. B. Kinetic Theory of Fibrillogenesis of Amyloid β-Protein. *Proc. Natl. Acad. Sci. USA* **1997**, *94*, 7942.

[10] Kashchiev, D.; Auer, S. Nucleation of Amyloid Fibrils. *J. Chem. Phys.* **2010**, *132*, 215101.

[11] Kashchiev, D.; Cabriolu, R.; Auer, S. Confounding the Paradigm: Peculiarities of Amyloid Fibril Nucleation. *J. Am. Chem. Soc.* **2013**, *135*, 1531.

[12] Jarrett, J. T.; Costa, P. R.; Griffin, R. G.; Lansbury, P. T. Models of the β Protein C-terminus: Differences in Amyloid Structure May Lead to Segregation of "Long" and "Short" Fibrils. *J. Am. Chem. Soc.* **1994**, *116*, 9741.

[13] O'Nuallain, B.; Shivaprasad, S.; Kheterpal, I.; Wetzel, R. Thermodynamics of Aβ(1-40) Amyloid Fibril Elongation. *Biochemistry* **2005**, *44*, 12709.

[14] Garai, K.; Sahoo, B.; Sengupta, P.; Maiti, S. Quasihomogeneous Nucleation of Amyloid Beta Yields Numerical Bounds for the Critical Radius, the Surface Tension, and the Free Energy Barrier for Nucleus Formation. *J. Chem. Phys.* **2008**, *128*, 045102.

[15] Hellstrand, E.; Boland, B.; Walsh, D. M.; Linse, S. Amyloid β-Protein Aggregation Produces Highly Reproducible Kinetic Data and Occurs by a Two-Phase Process. *ACS Chem. Neurosci.* **2010**, *1*, 13.

[16] Baldwin, A. J.; Knowles, T. P. J.; Tartaglia, G. G.; Fitzpatrick, A. W.; Devlin, G. L.; Shammas, S. L.; Waudby, C. A.; Mossuto, M. F.; Meehan, S.; Gras, S. L. et al. Metastability of Native Proteins and the Phenomenon of Amyloid Formation. *J. Am. Chem. Soc.* **2011**, *133*, 14160.

[17] Davies, R. P. W.; Aggeli, A. Self-Assembly of Amphiphilic β-Sheet Peptide Tapes Based on Aliphatic Side Chains. *J. Pept. Sci.* **2011**, *17*, 107–114.

[18] Yagi, H.; Hasegawa, K.; Yoshimura, Y.; Goto, Y. Acceleration of the Depolymerization of Amyloid β-Fibrils by Ultrasonication. *Biochimica et Biophysica Acta* **2013**, *1834*, 2480.

[19] Harper, J. D.; Lansbury, P. T. Models of Amyloid Seeding in Alzheimer's Disease and Scrapie: Mechanistic Truths and Physiological Consequences of the Time-Dependent Solubility of Amyloid Proteins. *Annu. Rev. Biochem.* **1997**, *66*, 385.

[20] Wood, S. J.; Wetzel, R.; Martin, J. D.; Hurle, M. R. Prolines and Amyloidogenicity in Fragments of the Alzheimer's Peptide βA4. *Biochemistry* **1995**, *34*, 724.

[21] Wurth, C.; Guimard, N. K.; Hecht, M. H. Mutations That Reduce Aggregation of the Alzheimer's Aβ42 Peptide: An Unbiased Search for the Sequence Determinants of Aβ Amyloidogenesis. *J. Mol. Biol.* **2002**, *319*, 1279.

[22] Williams, A. D.; Shivaprasad, S.; Wetzel, R. Alanine Scanning Mutagenesis of Aβ(1-40) Amyloid Fibril Stability. *J. Mol. Biol.* **2006**, *357*, 1283.

[23] Kodali, R.; Williams, A. D.; Chemuru, S.; Wetzel, R. Aβ(1-40) Forms Five Distinct Amyloid Structures Whose β-sheet Contents and Fibril Stabilities Are Correlated. *J. Mol. Biol.* **2010**, *401*, 503.

[24] Qiang, W.; Kelley, K.; Tycko, R. Polymorph-Specific Kinetics and Thermodynamics of β-Amyloid Fibril Growth. *J. Am. Chem. Soc.* **2013**, *135*, 6860.

[25] Ferrone, F. A. Analysis of Protein Aggregation Kinetics. *Methods Enzymol.* **1999**, *309*, 256.

[26] Schreck, J. S.; Yuan, J.-M. Statistical Mechanical Treatments of Protein Amyloid Formation. *Int. J. Mol. Sci.* **2013**, *14*, 17420.

[27] DuBay, K. F.; Pawar, A. P.; Chiti, F.; Zurdo, J.; Dobson, C. M.; Vendruscolo, M. Prediction of the Absolute Aggregation Rates of Amyloidogenic Polypeptide Chains. *J. Mol. Biol.* **2004**, *341*, 1317.

[28] Fernandez-Escamilla, A.; Rousseau, F.; Schymkowitz, J.; Serrano, L. Prediction of Sequence-Dependent and Mutational Effects on the Aggregation of Peptides and Proteins. *Nature Biotech.* **2004**, *22*, 1302.

[29] Conchillo-Solé, O.; de Groot, N. S.; Avilés, F. X.; Vendrell, J.; Daura, X.; Ventura, S. AGGRESCAN: A Server for the Prediction and Evaluation of "Hot Spots" of Aggregation in Polypeptides. *BMC Bioinfo.* **2007**, *8*, 65.

[30] Tartaglia, G. G.; Pawar, A. P.; Campioni, S.; Dobson, C. M.; Chiti, F.; Vendruscolo, M. Prediction of Aggregation-Prone Regions in Structured Proteins. *J. Mol. Biol.* **2008**, *380*, 425.

[31] Wu, C.; Shea, J.-E. Coarse-Grained Models for Protein Aggregation. *Curr. Opin. Struct. Biol.* **2011**, *21*, 209.

[32] Morriss-Andrews, A.; Shea, J.-E. Simulations of Protein Aggregation: Insights From Atomistic and Coarse-Grained Models. *J. Phys. Chem. Lett.* **2014**, *5*, 1899.

[33] Nguyen, H. D.; Hall, C. K. Phase Diagrams Describing Fibrillization by Polyalanine Peptides. *Biophys. J.* **2004**, *87*, 4122.

[34] Nguyen, H. D.; Hall, C. K. Spontaneous Fibril Formation by Polyalanines; Discontinuous Molecular Dynamics Simulations. *J. Am. Chem. Soc.* **2006**, *128*, 1890.

[35] Ricchiuto, P.; Brukhno, A. V.; Auer, S. Protein Aggregation: Kinetics Versus Thermodynamics. *J. Phys. Chem. B* **2012**, *116*, 8703.

[36] Auer, S.; Kashchiev, D. Phase Diagram of α-Helical and β-Sheet Forming Peptides. *Phys. Rev. Lett.* **2010**, *104*, 168105.

[37] Auer, S. Phase Diagram of Polypeptide Chains. *J. Chem. Phys.* **2011**, *135*, 175103.

[38] Ni, R.; Abeln, S.; Schor, M.; Stuart, M. A. C.; Bolhuis, P. G. Interplay Between Folding and Assembly of Fibril-Forming Polypeptides. *Phys. Rev. Lett.* **2013**, *111*, 058101.

[39] Zhang, J.; Muthukumar, M. Simulations of Nucleation and Elongation of Amyloid Fibrils. *J. Chem. Phys.* **2009**, *130*, 035102.

[40] Cabriolu, R.; Kashchiev, D.; Auer, S. Breakdown of Nucleation Theory for Crystals with Strongly Anisotropic Interactions Between Molecules. *J. Chem. Phys.* **2012**, *137*, 204903.

[41] Bingham, R. J.; Rizzi, L. G.; Cabriolu, R.; Auer, S. Non-Monotonic Supersaturation Dependence of the Nucleus Size of Crystals with Anisotropically Interacting Molecules. *J. Chem. Phys.* **2013**, *139*, 241101.

[42] Irbäck, A.; Jonsson, S.; Linnemann, N.; Linse, B.; Wallin, S. Aggregate Geometry in Amyloid Fibril Nucleation. *Phys. Rev. Lett.* **2013**, *110*, 058101.

[43] Irbäck, A.; Wessén, J. Thermodynamics of Amyloid Formation and the Role of Intersheet Interactions. *J. Chem. Phys.* **2015**, *143*, 105104.

[44] Cabriolu, R.; Auer, S. Amyloid Fibrillation Kinetics: Insight From Atomistic Nucleation Theory. *J. Mol. Biol.* **2011**, *411*, 275.

[45] Auer, S. Nucleation of Polymorphic Amyloid Fibrils. *Biophys. J.* **2015**, *108*, 1176.

[46] Haas, C.; Drenth, J. The Interaction Energy Between Two Protein Molecules Related to Physical Properties of Their Solution and Their Crystals and Implications for Crystal Growth. *J. Cryst. Growth* **1995**, *154*, 126.

[47] Rizzi, L. G.; Head, D. A.; Auer, S. Universality in the

Morphology and Mechanics of Coarsening Amyloid Fibril Networks. *Phys. Rev. Lett.* **2015**, *114*, 078102.

[48] Sawaya, M. R.; Sambashivan, S.; Nelson, R.; Ivanova, M. I.; Sievers, S. A.; Apostol, M. I.; Thompson, M. J.; Balbirnie, M.; Wiltzius, J. J. W.; McFarlane, H. T. et al. Atomic Structures of Amyloid Cross-β Spines Reveal Varied Steric Zippers. *Nature* **2007**, *447*, 453.

[49] Fitzpatrick, A. W. P.; Debelouchina, G. T.; Bayro, M. J.; Claire, D. K.; Caporini, M. A.; Bajaj, W. S.; Jaroniec, C. P.; Wang, L.; Ladizhansky, V.; Müller, S. A. et al. Atomic Structure and Hierarchical Assembly of a Cross-β Amyloid Fibril. *P. Natl. Acad. Sci. USA* **2013**, *110*, 5468.

[50] Auer, S. Amyloid Fibril Nucleation: Effect of Amino Acid Hydrophobicity. *J. Phys. Chem. B* **2014**, *118*, 5289.

[51] Ferrone, F. A. Assembly of Aβ Proceeds via Monomeric Nuclei. *J. Mol. Biol.* **2015**, *427*, 287.

[52] Chiti, F.; Stefani, M.; Taddei, N.; Ramponi, G.; Dobson, C. M. Rationalization of the Effects of Mutations on Peptide and Protein Aggregation Rates. *Nature* **2003**, *424*, 805.

[53] Chiti, F.; Taddei, N.; Baroni, F.; Capanni, C.; Stefani, M.; Ramponi, G.; Dobson, C. M. Kinetic Partitioning of Protein Folding and Aggregation. *Nat. Struct. Biol.* **2002**, *9*, 137.

[54] de Groot, N. S.; Aviles, F. X.; Vendrell, J.; Ventur, S. Mutagenesis of the Central Hydrophobic Cluster in Aβ42 Alzheimer's Peptide Side-Chain Properties Correlate with Aggregation Propensities. *FEBS Journal* **2006**, *273*, 658.

[55] Cheng, P. N.; Pham, J. D.; Nowick, J. S. The Supramolecular Chemistry of β-Sheets. *J. Am. Chem. Soc.* **2011**, *135*, 5477.

[56] Meersman, F.; Dobson, C. M. Probing the Pressure-Temperature Stability of Amyloid Fibrils Provides New Insights into Their Molecular Properties. *Biochimica et Biophysica Acta* **2006**, *1764*, 452.

[57] Hamley, I. W.; Nutt, D. R.; Brown, G. D.; Miravet, J. F.; Escuder, B.; Rodríguez-Llansola, F. Influence of the Solvent on the Self-Assembly of a Modified Amyloid Beta Peptide Fragment. II. NMR and Computer Simulation Investigation. *J. Phys. Chem. B* **2010**, *114*, 940.